Protein Science (2000), *9*:2232–2245. Cambridge University Press. Printed in the USA.

Trp42 rotamers report reduced flexibility when the inhibitor acetyl-pepstatin is bound to HIV-1 protease

BEÁTA ULLRICH,[1] MONIQUE LABERGE,[1] FERENC TÖLGYESI,[1] ZOLTÁN SZELTNER,[2] LÁSZLÓ POLGÁR,[2] AND JUDIT FIDY[1]

[1]Institute of Biophysics and Radiation Biology, Semmelweis University, P.O.B. 263 H-1444 Budapest, Hungary
[2]Institute of Enzymology, Biological Research Centre, Hungarian Academy of Sciences, P.O.B. 7, H-1518 Budapest, Hungary

(RECEIVED January 25, 2000; FINAL REVISION August 15, 2000; ACCEPTED August 24, 2000)

Abstract

The Q7K/L33I/L63I HIV-1 protease mutant was expressed in *Escherichia coli* and the effect of binding a substrate-analog inhibitor, acetyl-pepstatin, was investigated by fluorescence spectroscopy and molecular dynamics. The dimeric enzyme has four intrinsic tryptophans, located at positions 6 and 42 in each monomer. Fluorescence spectra and acrylamide quenching experiments show two differently accessible Trp populations in the apoenzyme with $k_{q1} = 6.85 \times 10^9\ M^{-1}\,s^{-1}$ and $k_{q2} = 1.88 \times 10^9\ M^{-1}\,s^{-1}$, that merge into one in the complex with $k_q = 1.78 \times 10^9\ M^{-1}\,s^{-1}$.

500 ps trajectory analysis of Trp χ_1/χ_2 rotameric interconversions suggest a model to account for the observed Trp fluorescence. In the simulations, Trp6/Trp6B rotameric interconversions do not occur on this timescale for both HIV forms. In the apoenzyme simulations, however, both Trp42s and Trp42Bs are flipping between χ_1/χ_2 states; in the complexed form, no such interconverions occur. A detailed investigation of the local Trp environments sampled during the molecular dynamics simulation suggests that one of the apoenzyme Trp42B rotameric interconversions would allow indole-quencher contact, such as with nearby Tyr59. This could account for the short lifetime component. The model thus interprets the experimental data on the basis of the conformational fluctuations of Trp42s alone. It suggests that the rotameric interconversions of these Trps, located relatively far from the active site and at the very start of the flap region, becomes restrained when the apoenzyme binds the inhibitor. The model is thus consistent with associating components of the fluorescence decay in HIV-1 protease to ground state conformational heterogeneity.

Keywords: 500 ps molecular dynamics; acrylamide quenching; dihedral trajectories; dynamics influenced by inhibitor; ground state heterogeneity; Trp fluorescence; Trp rotamers

HIV-1 protease the homodimeric aspartyl-protease encoded in the viral genome of the HIV-1 virus is essential for the proper maturation of the virus. It cleaves the polyprotein products of the *gag* and *pol* viral genes (Kohl et al., 1988), making the release of enzyme proteins including the protease itself possible (Seelmeier et al., 1988). Inactivation of the enzyme by mutation or chemical inhibition causes the production of immature, noninfectious viral particles (Seelmeier et al., 1988). Use of the enzyme was proposed as a target in anti-AIDS drug design, and thus the effect of binding various inhibitors on protease structure and activity is currently the focus of intensive research (Fitzgerald et al., 1990; Wlodawer & Erickson, 1993; Pargellis et al., 1994; Polgár et al., 1994; Yamazaki et al., 1994; Nicholson et al., 1995; Wlodawer & Vondrasek, 1998; Trylska et al., 1999). Four such inhibitors, i.e., saquinavir, indinavir, ritonavir, and nelfinavir, were recently introduced to clinical applications (Flexner, 1998), as a result of structure assisted drug design (Wlodawer & Vondrasek, 1998). While a great amount of effort has been invested toward practical applications (e.g., determination of inhibitor binding constants, description of the active site triad), little has been contributed to the detailed understanding of the structural consequences of inhibitor binding at the level of the whole protein molecule. To obtain information about the structure of the enzyme in solution, NMR spectroscopy has been used for several years, but no results have been published about the apoenzyme itself, the studies being limited to the protease complex with various inhibitors (Yamazaki et al., 1994; Wang et al., 1996a, 1996b). The lack of comparative studies is probably due to the fact that the apoenzyme is known to undergo autoproteolysis (Rosé et al., 1993; Mildner et al., 1994). In the present study, we focused our interest on complex formation with acetyl-pepstatin and used the Q7K/L33I/L63I HIV-1 mutant, known to be resistant to autoproteolysis (Mildner et al., 1994). Highly sensitive fluorescence spectroscopic methods allowed us to perform the studies in solutions of low concentration.

There are three available crystal structures for HIV-1 protease, determined at various resolutions: the α-carbon backbone structure

Reprint requests to: Judit Fidy, Institute of Biophysics and Radiation Biology, Semmelweis University, P.O.B. 263 H-1444 Budapest, Hungary; e-mail: judit@puskin.sote.hu.

of the NY5 isolate at 3.0 Å (Navia et al., 1989), the synthetic structure replacing two cysteines by ABAs at 2.8 Å (Wlodawer et al., 1989), and the 2.7 Å structure of the native protease (Lapatto et al., 1989). The coordinates of several protease complexes with peptide or nonpeptide inhibitors have also been deposited at the Protein Data Bank (PDB), including the 2.0 Å resolution structure of HIV-1 complexed to acetyl-pepstatin (Fitzgerald et al., 1990), as well as that of the Q7K/L33I/L63I mutant complexed to the Glu-Asp-Leu tripeptide (2 Å, Louis et al., 1998).

HIV-1 protease is a dimer (Fig. 1A), containing two identical subunits and two Trp residues per monomer, at positions 6 and 42. The greater part of the protease is ordered in β-strands except for residues 86–94, which are ordered in α-helical form. Asp25, Thr26, and Gly27 form the "active site triad" at the dimer interface where the inhibitor binds. The binding site can accommodate six to eight amino acid residues. Residues 42–58 form a highly flexible region in each subunit of the protease, referred to as the "flap region." It is also part of the dimer interface and it is evident from the X-ray structures that it is significantly involved in the conformational change occurring upon inhibitor binding. A 4.6 Å motion of the flap region toward the active site takes place upon binding, as seen in the upper part of the structures shown in Figure 1. The monomers are slightly asymmetric, as illustrated in Table 1, which lists some inequivalent distances measured from Trp residues in the two subunits of the complex. The two Trp residues (6 and 42, respectively) are also not equivalent, both in terms of geometry and in the respective environments in which they are found: Trp6—located close to the N-terminal believed to play a role in the H-bond network connecting the two monomers (York et al., 1993)—stretches out in solvent (cf. Fig. 2), while Trp42, located in the flap region, has its aromatic ring flipped back unto itself and in closer contact with the protein matrix. The above differences between Trp6 and Trp42 are maintained in both the complexed and uncomplexed forms of HIV-1.

Table 1. *Inequivalent atomic distances between residues in the two subunits of the HIV-1 complex with acetyl pepstatin*[a]

Trp	Residue	Distance (Å)	Trp	Residue	Distance (Å)	Difference (Å)
6	Asn37B	31.99	6B	Asn37	30.01	1.98
6	Lys7	7.41	6B	Lys7B	9.76	2.35
6	Lys7B	29.33	6B	Lys7	27.34	1.99
6	Gln92B	10.03	6B	Gln92	6.80	3.23
42	Glu65	24.45	42B	Glu65B	26.42	1.97
42	Glu35B	38.90	42B	Glu35	36.23	2.67
42	Asn37	9.12	42B	Asn37B	11.64	2.52

[a]The atomic distances were measured between the indole N of Trp and the γ-C in case of Asn and δ-C atoms in cases of Glu and Gln.

The presence of tryptophan intrinsic probes makes the protease a good candidate for fluorescence studies. Conformational changes caused by increased pH and Mg(II) ion concentration were successfully monitored using the emission spectrum of the intrinsic Trp residues (Tyagi et al., 1994). In a recent work, the fluorescence intensity and anisotropy decay of several apoenzyme–inhibitor complexes were studied using a ps laser excitation technique, and the lifetime components extracted from the fluorescence decay mea-

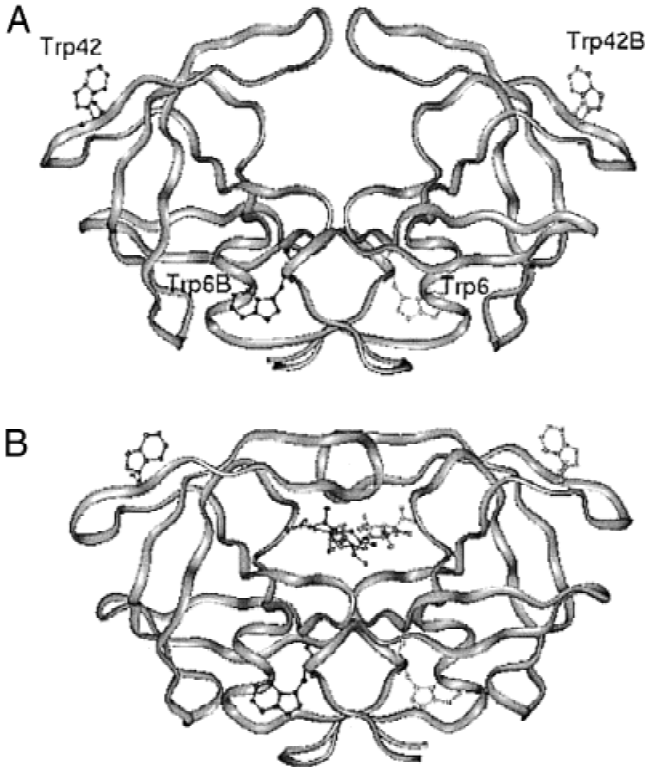

Fig. 1. Structure of (**A**) HIV-1 protease and (**B**) its complex with acetyl pepstatin. The Trp residues and the inhibitor are rendered as balls and sticks.

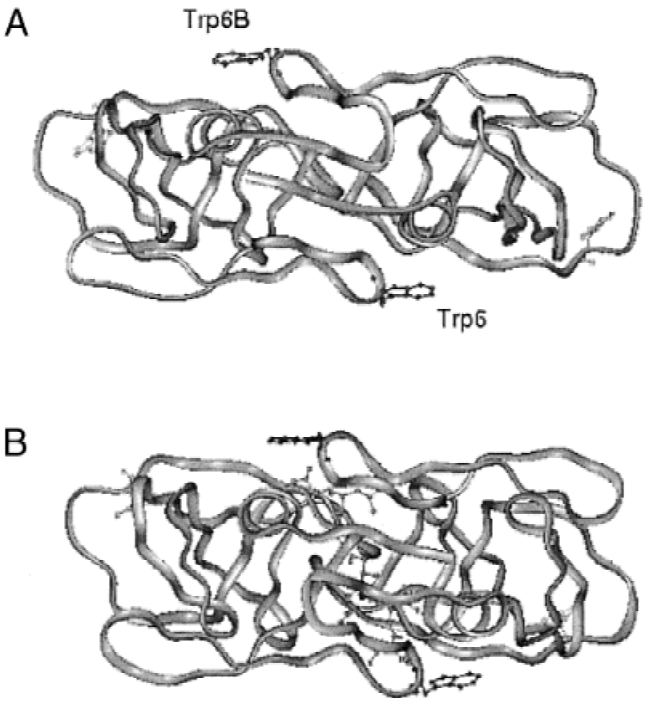

Fig. 2. Side view of (**A**) the structures of HIV-1 protease and (**B**) its complex with acetyl pepstatin.

surements were identified based on simulations of the dynamic behavior of the two types of Trp residues present in the structure (Kungl et al., 1998; Ringhofer et al., 1999). The complex with the inhibitor acetyl-pepstatin has not been studied previously.

In this work, we compare the structure of the Q7K/L33I/L63I mutant HIV1-protease and its complex with acetyl-pepstatin. We present models for the structure of the mutant apoenzyme obtained from the three-dimensional (3D) structural data available for its complex with a small tripeptide inhibitor. We describe the dynamic behavior of the Trp residues during the course of comparative 500 ps molecular dynamics simulations (MDS) and propose a model to interpret the ns-experimental fluorescence data on the basis of Trp42B rotamer states exploring different local environments. We compare their respective accessibility to potential quencher groups and discuss the different local environments of Trp6s and Trp42s.

Results

Fluorescence spectroscopy and excited state lifetime

The corrected and normalized fluorescence excitation and emission spectra of the apoenzyme at room temperature are shown in Figure 3A. Complex formation does not influence the fluorescence emission spectra significantly, thus it is not shown in the figure. Figure 3B shows the fluorescence excitation spectra of the enzyme and that of the complex overlaid. This shows a significant difference in the blue side of the excitation maximum where the contribution of the $L_a \leftarrow {}^1A$ transition is known to predominate (Callis, 1997; Valeur & Weber, 1977).

In Figure 4A, the fluorescence decay of the apoenzyme is shown at room temperature, as registered by the ns-flashlamp system, with excitation at 295 nm and emission at 340 nm. The decay curves could not be well fitted with one exponential, but the sum of two exponentials resulted in acceptable chi-squared values (cf. weighted residuals in the figure). In the case of the complex (Fig. 4B), the two exponential fit did not improve the quality of the fit significantly. The data (average values of several independent experimental series) are shown in Table 2. For the apoenzyme, typical values from the two-component fit were: τ_1 = 2.73 ns (19.2%) and τ_2 = 5.7 ns (80.8%), $\langle\tau\rangle$ = 5.13 ns and for the complex: τ_1 = 3.1 ns (21.7%) and τ_2 = 5.9 ns (78.3%), $\langle\tau\rangle$ = 5.29 ns.

Fluorescence quenching studies

Effect on the spectra

Fluorescence quenching studies using acrylamide as a quencher were performed to test if the two discrete lifetime components of the fluorescence decay can be identified as the contribution of two

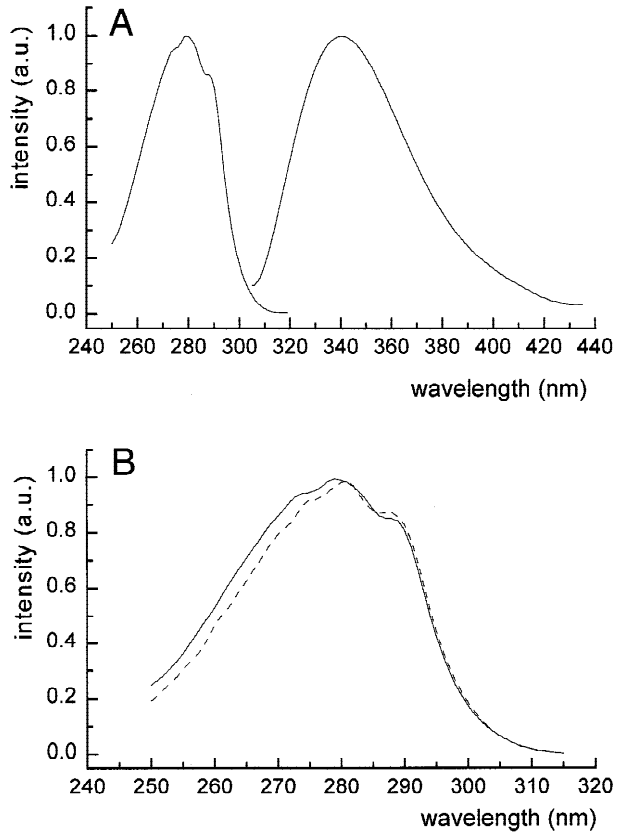

Fig. 3. A: Fluorescence excitation (λ_{em} = 340 nm) and emission (excitation λ_{ex} = 295 nm) spectra of the apoenzyme. **B:** Superposed excitation spectra of apoenzyme and complex (dashed line).

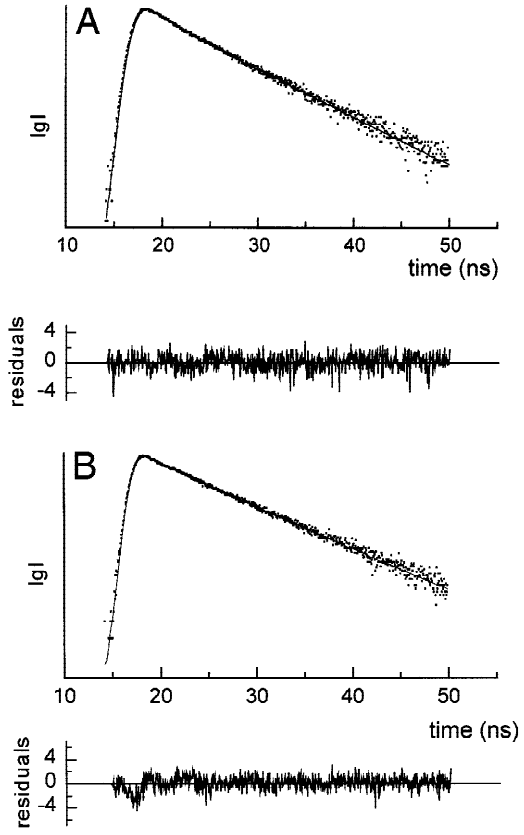

Fig. 4. Fluorescence decay of (**A**) the apoenzyme and (**B**) the complex. Decays were collected at 295 nm of excitation wavelength and 340 nm of emission wavelength. Results of two-exponential fits for the presented decays were: τ_1 = 2.7 ns, f_1 = 19.7%, τ_2 = 5.6 ns, f_2 = 80.3%, (apoenzyme), τ_1 = 3.36 ns, f_1 = 19.9%, τ_2 = 5.84 ns, f_2 = 80.1%.

Table 2. *Van der Waal contact with protein quencher groups by the different Trp rotamers sampled during 500 ps simulation time*

		ApoHIV-1		Complex	
			vdW contact		vdW contact
Trp6	χ_1	g^-	N	g^-	N
	χ_2	$-90°$	N	$-90°$	N
Trp6B	χ_1	g^-	N	g^-	N
	χ_2	$-90°$	N	$-90°$	N
Trp42	χ_1	g^+	N	g^+	N
	χ_2	$90/-90°$	N	$90°$	N
Trp42B	χ_1	g^+/g^-	Y	g^+	N
	χ_2	$90/-90°$	Y	$90°$	N

differently accessible Trps of the protein. We selected acrylamide as quencher because it only has a very slight effect on the enzyme activity of HIV-1 protease (3–5% decrease at a 0.3 M acrylamide concentration). Similar concentrations of iodide as quencher drastically lowered the enzyme activity.

The fluorescence intensity at a constant emission wavelength (λ_{ex} = 295 nm, λ_{em} = 340 nm) as well as emission spectra (λ_{ex} = 295 nm) were measured as described in Materials and methods. The intensity plot, shown in Figure 5, shows a downward curvature in the case of the apoenzyme. The same experiment in the case of the complex leads to an upward-curving intensity plot (cf. Fig. 5). A Lehrer plot analysis (not shown) was also performed, based on the most simple model, i.e., that the emission occurs from one

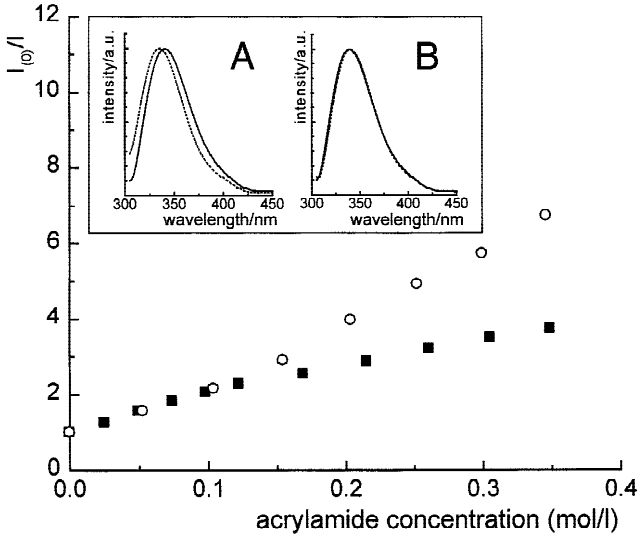

Fig. 5. Intensity Stern–Volmer plots of the apoenzyme (■) and the complex (○). Inset: Fluorescence emission spectra of (**A**) the apoenzyme and (**B**) the complex at 0 M (solid line) and 0.35 M (dashed line) acrylamide concentrations, excitation wavelength = 295 nm.

accessible and one inaccessible Trp, using the linearized form of the Stern–Volmer equation (Lehrer, 1971):

$$\frac{I_0}{\Delta I} = \frac{1}{f_a K_D [Q]} + \frac{1}{f_a} \quad (1)$$

where f_a is the fraction of the initial fluorescence that is accessible to the quencher and ΔI is the difference between the intensity of fluorescence in the absence of quencher (I_0) and the intensity at various quencher concentrations. The linear fit to $I_0/\Delta I$ plotted as a function of $[Q]$ (not shown) yielded 86% for the contribution of the accessible Trps in the apoenzyme and around 100% for the complex (i.e., the *y*-intercept was close to 1).

The downward curvature of the Stern–Volmer plot in the case of the apoenzyme agrees well with the multicomponent feature of the lifetime data. It indicates that there are Trps in the protein with distinct accessibility for quenching (Eftink & Ghiron, 1981). The inset of Figure 5 shows that quenching leads to a blue shift in the emission spectrum of the apoenzyme. This result is not only indicative of the presence of distinct Trps, but also shows that the Trps with red shifted spectra are more effectively quenched.

In the case of the complex, no significant spectral change could be observed upon quenching (cf. Fig. 5, inset). Thus, the Trps in this conformation are not significantly different in their accessibility for quenching. The upward curvature observed in the intensity plot of the quenching experiment is probably indicative of the occurrence of both dynamic and static processes, but a similar effect arising from a significant contribution of the transient term of the Smoluchowski equation (Eftink & Ghiron, 1981) during the quenching process cannot be excluded either.

Effect on the fluorescence decay

Figure 6A shows a Stern–Volmer plot based on an evaluation using two lifetime components for the case of the apoenzyme. It is seen that both lifetime components can be fitted to linear plots, yielding significantly distinct k_q bimolecular quenching constants. The values are listed in Table 3. The conclusion from the quenching studies for the apoenzyme is that the data can be well interpreted by assuming the existence of two types of Trp populations. The population with shorter lifetime is more effectively quenched by a collisional mechanism, and this population has emission spectra red shifted relative to that of longer lifetime.

In the case of the complex, the decay curves could not be so well fitted by two lifetimes (as mentioned above). The Stern–Volmer plots based on two lifetime components did not lead to straight lines (not shown), but a downward curvature could be observed. As the intensity plot and the spectral data shown in Figure 5 were indicative of similar Trp behavior in the quenching experiment, we evaluated the lifetime data by using the mean lifetime in the Stern–Volmer plot as shown in Figure 6B. The data points are from three independent experiments; they can be well fitted by a straight line. The bimolecular quenching constant is given in Table 3; it is somewhat smaller than that of the Trps with longer lifetime components in the apoenzyme.

Trp dynamics by computer simulations

Figures 7 and 8 plot the variation of the χ_1 and χ_2 Trp dihedral angles for the 500 ps time course of the distance-dependent dielectric simulations acquired after a 100 ps equilibration. All Trp

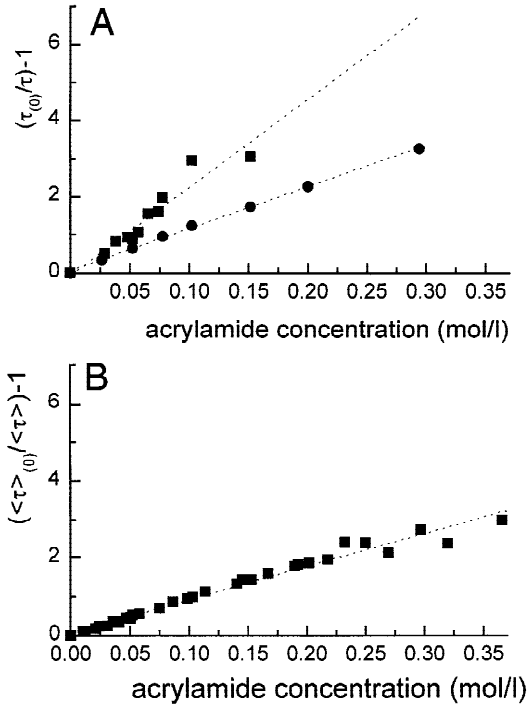

Fig. 6. Stern–Volmer plots for τ_1 (■) and τ_2 (●) discrete lifetime components of (**A**) the apoenzyme and (**B**) for $\langle\tau\rangle$ data of the complex. Excitation wavelength = 295 nm; emission wavelength = 340 nm.

residues are seen to adopt the χ_1/χ_2 geometries of stereochemically favored staggered rotamers, i.e., g^+, g^-, or 90° or −90° (cf. Materials and methods). The distribution of rotamer populations is also listed in Table 2. We note here that Trp does not adopt the third possible χ_1 rotamer, i.e., $t = 180°$; this is not surprising as this rotamer has been shown to be indicative of α-helical structure (Willis et al., 1994), which does not occur in this region of the protease.

The most dynamically active Trp is Trp42B, which switches between two possible χ_1/χ_2 rotamers, but only in the apoenzyme (cf. bottom left graphs in Figs. 7, 8). In the complex, it adopts only one χ_1/χ_2 conformation (cf. bottom right graphs in Figs. 7, 8). As for Trp42, it adopts the g^+ geometry in both the apoenzyme and the complex, and both 90°/−90° conformations in the apoenzyme. We note here that this type of dynamic behavior was observed in both explicitly solvated and distance-dependent dielectric simulations for the length of available and comparable trajectory time (cf. Materials and methods). In the motion of Trp6 and Trp6B, the trajectories did not show significant differences, both in the apoenzyme and in the complex. These residues kept fluctuating about the same average geometry, i.e., that of the g^+ for the χ_1, and 90° for the χ_2 dihedral case.

To illustrate how the rotamer conformations sampled by the Trp residues during the time course of the trajectories report on the local protein environment, we display graphically (Figs. 9, 10) the proximity of the Trp indoles to a protein matrix quencher group, i.e., the phenol group of Tyr59 (Chen & Barkley, 1998). For clarity's sake, we only display the van der Waals surfaces of the strongest quencher present in the respective environments of the Trp residues. Specifically, Figure 9 compares—for both apoenzyme and complex—the quenching environment of Trp42 and Trp42B in the χ_1 rotamer conformations extracted from the MDS and shows that, in its "flipping" motion between two rotamers, Trp42Bg^- in the apoenzyme is the only species which comes into effective van der Waals contact with the quencher. Figure 10 compares the χ_2 interconversions. In the case of the apoenzyme Trp42, the 90° and −90° rotamer interconversion does not bring the indole closer to the quencher (Fig. 10A,B). However, in the case of Trp42B (Fig. 10C,D), interconversion again results in van der Waals overlap of the −90° rotamer with the quencher group (Fig. 10D).

Thus, the dynamics are suggestive of two different Trp42 populations: one that would make van der Waals contact with a quenching group, consisting of the −90° and g^- rotamers of Trp42B exposed to quencher in the apoenzyme, and another population, not exposed to Tyr59, that would consist of Trp42 in both apoenzyme and complex and of the 90° and g^+ rotamers of Trp42B in the complex.

The same analysis was performed for all other known quencher groups of indole present within probable van der Waals overlap distance, i.e., the sulfhydryl group of Cys (no contact); the amide groups of Asn37, Asn37B, Asn88 (no contact), and of Gln58, 92B (no contact); the ϵ-amino group of Lys43, Lys55, and Lys55B (no contact). Special attention was paid to Lys7, which replaces Gln7 in the mutant protease. Its ϵ-amino group, also reported as an indole fluorescence quencher in this pH-range (Tran & Beddard, 1985), was observed to be dynamically quite active during the time course of the simulations, in some instances approaching Trp6 as close as 2.8 Å with van der Waals overlap of the residues. In the simulations, no other Lys residue was seen to approach a Trp indole so closely (e.g., Lys55, Lys55B, Lys43, Lys43B). The quenching mechanism of lysine in proteins is not yet known, but studies performed on model peptides (Chen & Barkley, 1998) have proposed an excited-state proton transfer mechanism. If this is the

Table 3. *Fluorescence decay parameters of apoenzyme and complex obtained from a double exponential fit*[a]

Apoenzyme			Complex			
τ_i (ns)	Contribution (%)	k_q ($M^{-1}s^{-1}$)	τ_i (ns)	Contribution (%)	$\langle\tau\rangle$ (ns)	k_q ($M^{-1}s^{-1}$)
2.7 ± 0.16	19.2	6.85×10^9	3.1 ± 0.36	21.7	5.29	1.78×10^9
5.7 ± 0.05	80.8	1.88×10^9	5.9 ± 0.14	78.3		

[a]The decays were collected at $\lambda_{ex} = 295$ nm and $\lambda_{em} = 340$ nm.

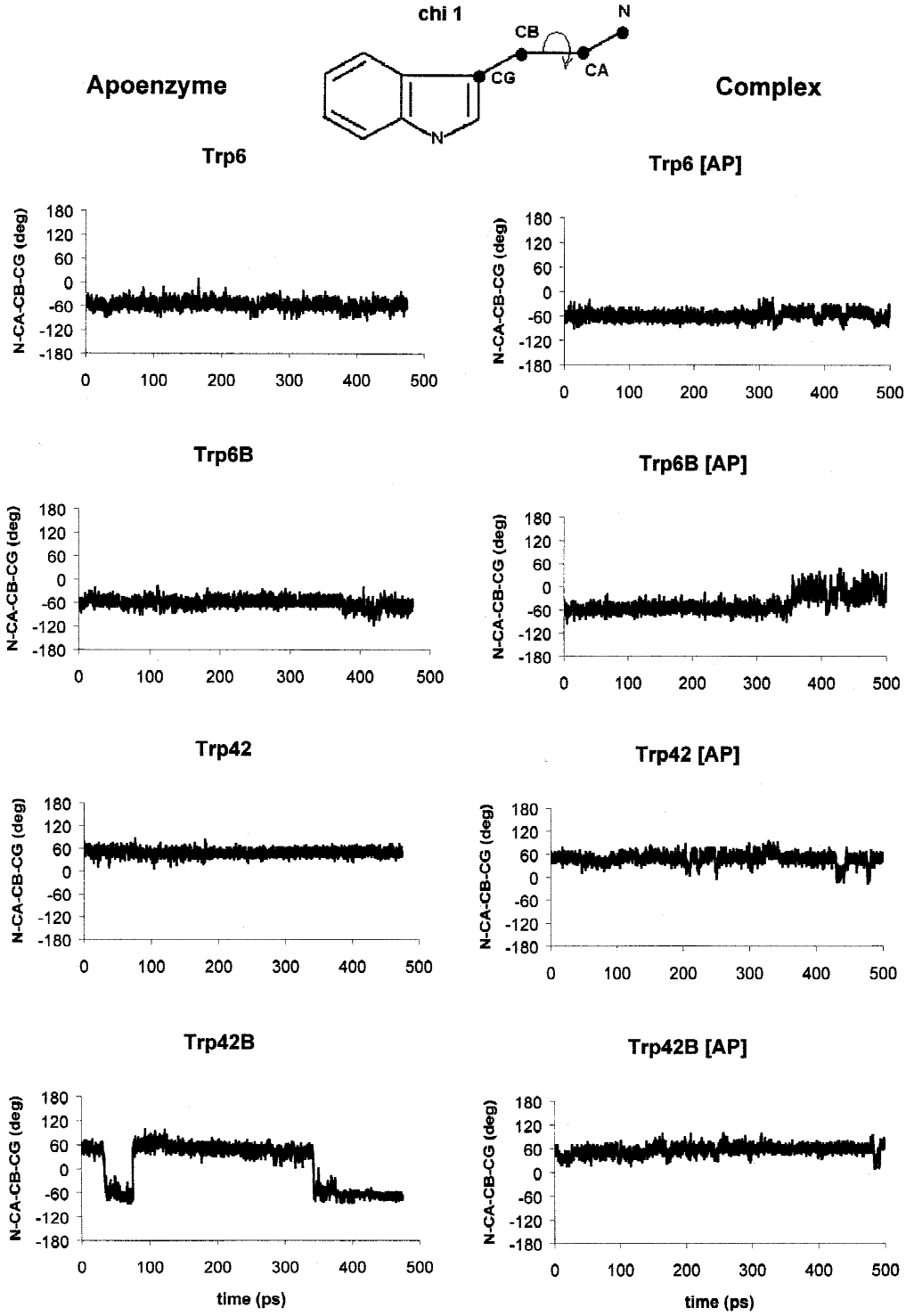

Fig. 7. Variation of the χ_1 dihedral angles of all four Trp residues (6, 6B, 42, and 42B) present in HIV-1 protease (left side) and in the complex (right side) during a 500 ps simulation. A dihedral of 60° corresponds to the g^+ rotamer and one of $-60°$ to the g^- rotamer. χ_1 is defined as the N-CA-CB-CG dihedral angle. AP symbol refers to the results obtained for the complex with acetyl-pepstatin inhibitor.

case, in addition to proximity, very stringent geometry orientations would also be required, so as to have the lysine make contact with either C2, C4, or C7 on the indole ring. No such overlap could be extracted from the MDS runs.

Possible peptide bond quenching was also investigated. In model peptide studies, effective quenching requires at least two amides (Chen et al., 1996), and such close overlap was not observed with backbone peptide bond segments in the immediate vicinity of the

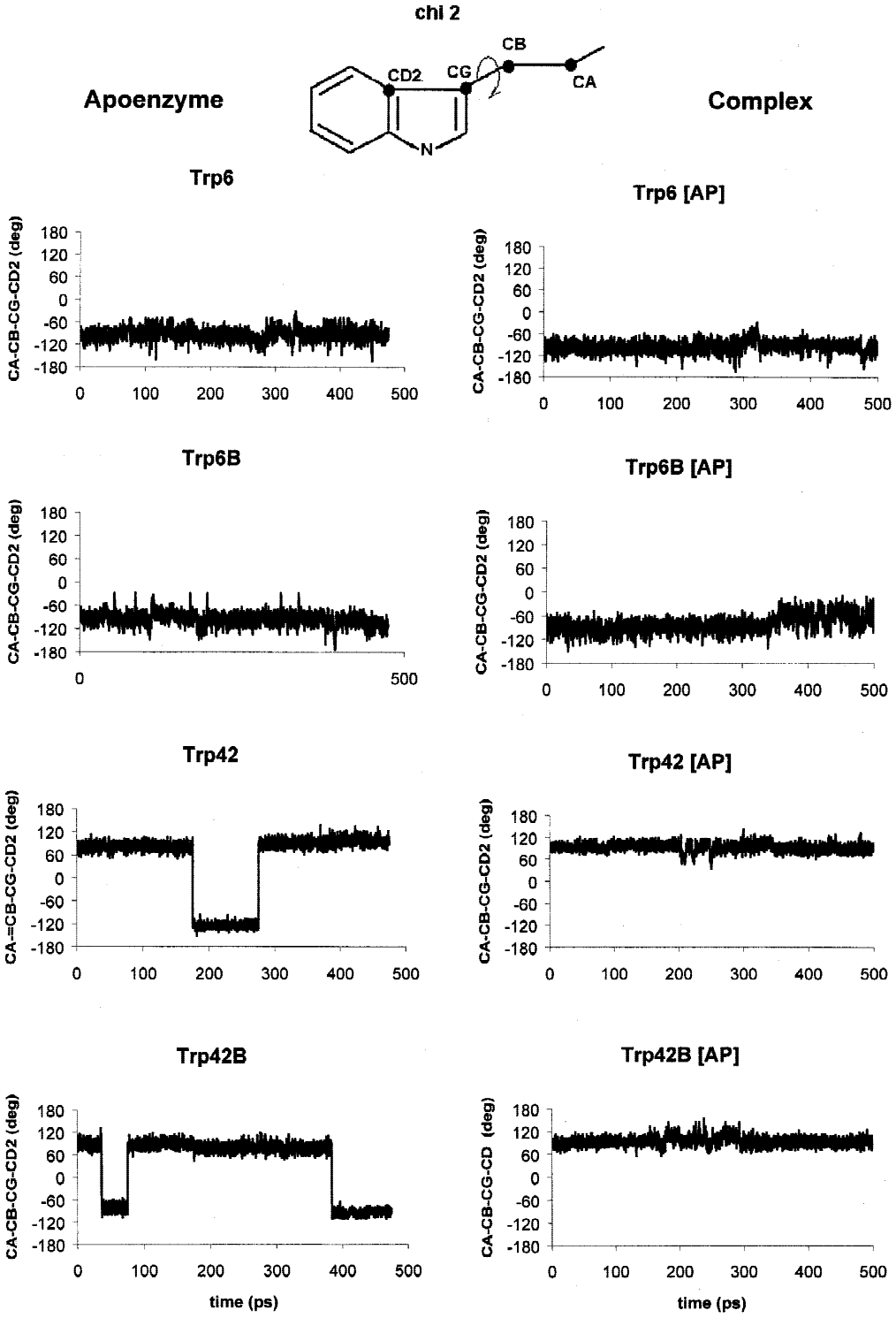

Fig. 8. Variation of the χ_2 dihedral angles of all four Trp residues (6, 6B, 42, and 42B) present in HIV-1 protease (left side) and in the complex (right side) during a 500 ps simulation. χ_1 is defined as the CA-CB-CG-CD2 dihedral angle. AP symbol refers to the results obtained for the complex with acetyl-pepstatin inhibitor.

Trps. However, recent work by Engelborgh's group shows that, in proteins, very effective quenching can occur by electron transfer from Trp's indole CE3 atom to Trp's own peptide bond—carbonyl carbon. Quenching can occur via a "through bond" mechanism; that is, the electron can travel along the covalent bond network linking the carbonyl C to the indole CE3 or via a "through space" pathway (Sillen et al., 2000). These quenching mechanisms, however, require specific orientations for the interacting orbitals. We

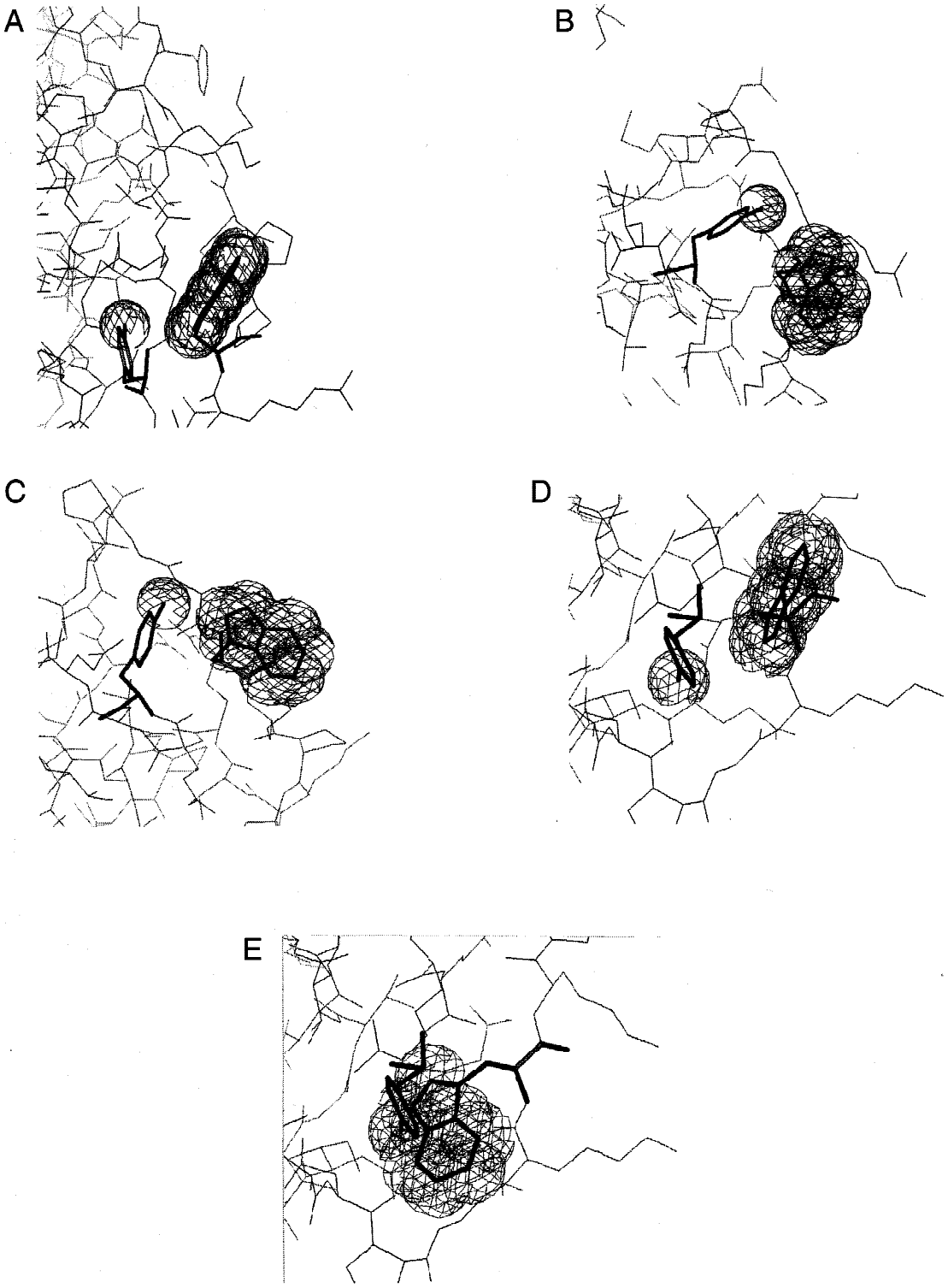

Fig. 9. Van der Waals surface renderings (mesh) of the χ_1 Trp rotamers and of the phenol of Tyr59 sampled during 500 ps and showing no quenching contact for a, b, c, and d (respectively, Trp42g$^+$ and Trp42Bg$^+$ in the complex, Trp42g$^+$ and B42g$^+$ in the apoprotease), and quenching overlap for e (Trp42Bg$^-$ in apo).

analyzed the trajectories to monitor the distance of the Trp indole CE3 atoms to the nearest peptide bond carbonyl C-atoms. This yielded distances that came within efficient quenching distance for the Trp42s but not for the Trp6s (~4.5 Å, cf. Sillen et al., 2000). However, even if the analysis resulted in showing that the distance requirement could be met, we could not investigate the orbital orientation requirement and could therefore not rigorously elaborate the details of a possible peptide bond additional quenching possibility.

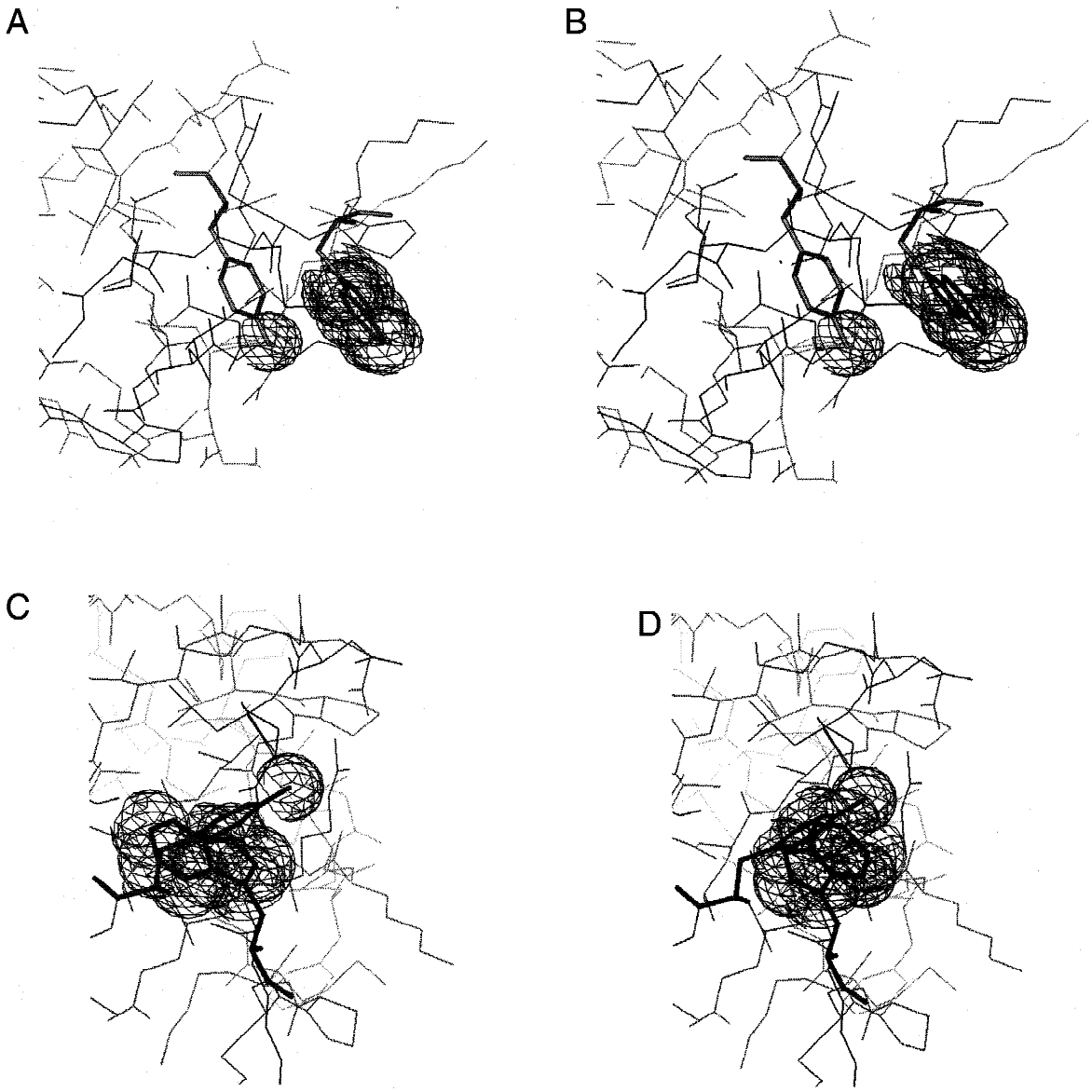

Fig. 10. Van der Waals surface renderings (mesh) of the χ_2 Trp rotamers and of the phenol of Tyr59 sampled during 500 ps and showing no quenching contact for the 90° and −90° rotamers of Trp42 and the 90° rotamer of Trp42B in the apoenzyme (**A**, **B**, and **C**) and quenching contact for the −90° rotamer of Trp42B in the apoenzyme (**D**).

Trp solvent accessible surfaces

The orientation of the protease structures (cf. Fig. 2) clearly shows that both Trp6 and Trp6B residues are solvated in the X-ray structures. It was of interest to know if this degree of solvation undergoes significant fluctuation extrema in time. The average SASA (cf. Materials and methods) calculated for all Trp residues in both complexed and uncomplexed forms during the 500 ps simulation are listed in Table 4 as well as the extreme maximum/minimum values. The Trp6 and Trp6B residues are seen to remain clearly solvated with *R* values consistently greater than 72.3, i.e., above the limiting value of 70 for solvent-exposed residues. The *R* values

Table 4. *Solvent accessible surface areas of Trp residues during 500 ps*

Trp	$R_{\text{HIV-1}}$ (R_{min}/R_{mx})	R_{Complex} (R_{min}/R_{mx})
6	77.2 (75.4/78.2)	74.8 (73.2/77.1)
6B	76.7 (75.1/79.0)	75.9 (72.3/76.7)
42	47.2 (44.4/49.5)	38.4 (36.9/43.1)
42B (g^+)	45.0 (42.7/46.3)	44.3 (41.2/47.8)
42B (g^-)	47.2 (43.4/48.2)	
42B (tr)	76.7 (72.6/78.2)	

of the Trp42 and of the Trp42B rotamers are also indicative of solvent exposure, but to a much lesser extent than the Trp6s with R values ≈40 (cf. R value for buried Trp is <20). They can thus be considered as partially buried or with one plane of the indole ring exposed to the protein matrix and the other to solvent. It should be noted that, in view of the simulations, as Trp42B flips from the g^+ to the g^- conformations, it also becomes fully solvent-exposed (42B"tr" in Table 4).

Discussion

Identification of the Trp fluorescence lifetime components

In the ns range, the fluorescence decay of the apoenzyme could be well fitted with two exponentials, namely 2.7 and 5.7 ns, with a much higher contribution from the longer component (cf. Table 2). The lifetime values are comparable to those reported by Kungl et al. (1998) for native HIV-1 protease. Those values were 2.06 and 4.46 ns, respectively. Besides the significant difference in the long lifetime, their respective contribution was also different, leading to an average lifetime of 2.23 ns. The cited study, however, is very different from ours, both in experimental methods and in studied samples (e.g., different pH, buffer, and wild-type enzyme). The authors used a frequency-doubled laser excitation source, and an analysis based on the maximum entropy method (MEM). The pulse shape shown in Figure 4 of their paper has a width of about 1 ns. It is evident that their method leads to a better signal/noise ratio and thus it allows for MEM analysis even for lifetime distributions centered around values in the ps range. The intrinsic time resolution of the experiment, however, does not improve much. The fact is that it would be hard to perform a precise comparative analysis of the two sets of results, even if the sample conditions had been identical.

In our quenching experiments, the validity of a heterogeneous source of emission is supported by the downward curvature of the Stern–Volmer intensity plot (Fig. 5), indicative of two populations not equally accessible to acrylamide. The dynamic collisional quenching constants k_q could reliably be determined for the two lifetime components, and they were very different (k_q values for the apoenzyme: $6.85 \times 10^9\ M^{-1}\,s^{-1}$ for τ_1 and $1.88 \times 10^9\ M^{-1}\,s^{-1}$ for τ_2). The short component is quenched with much higher efficiency by collision, and the spectra (cf. Fig. 5, inset) show that the accessible Trp residues in the system have moderately red-shifted emission (from 336 to 340 nm). From this, one has to conclude that the Trps of longer lifetime are in a relatively hydrophobic environment. As for the two quenching probabilities, one needs to consider especially the higher k_q value that is approaching the limiting value given for indole acrylamide quenching in water as $7 \times 10^9\ M^{-1}\,s^{-1}$ (Eftink & Ghiron, 1976). In the protein literature, however, one can find similar data: Bismuto and Irace (1994) report bimolecular quenching constants of even 8.9×10^9 and $2.3 \times 10^9\ M^{-1}\,s^{-1}$ for the acrylamide quenching of apomyoglobin Trps. More recently, a value of $6.4 \times 10^9\ M^{-1}\,s^{-1}$ was reported for the long component associated with a Trp nearly fully exposed to solvent in the smooth muscle myosin motor domain with the essential light chain (Yengo et al., 1999). Thus, we conclude that our values agree well with other reported data.

In the complex form, the two component fit of the fluorescence decay curves is somewhat questionable; the Stern–Volmer analysis of the quenching results also suggests that the two lifetime components have no real physical meaning. The same analysis, based on the mean lifetime (i.e., 5.29 ns), however, shows a linear dependence. There is also no spectral change due to the presence of the quencher. All these facts lead us to conclude that the probability of collisional quenching is very similar for all the Trps in the dimeric protein and that all have about the same fluorescence decay time. Thus, the binding of the inhibitor somewhat decreases the long lifetime component of the apoenzyme and significantly increases the short component.

The MDS trajectories suggest a model in which inhibitor binding would only affect the motion of Trp42B. In the trajectories, this Trp becomes very similar to that of Trp42 in the complex. Since Trp42 and Trp6 are located in very different environments (cf. Table 4), it is hard to imagine that they would form one population in the complex with respect to collisional quenching and fluorescence lifetime. Thus, a possible interpretation of our data would be that the contribution of Trp6 and Trp6B to the overall fluorescence decay is negligible on the ns timescale. In this interpretation, the effect of inhibitor binding would be based solely on the Trp42 rotamers with corresponding assignments that the 2.7 and 5.7 ns lifetimes characterize different rotameric states of Trp42 in the apoenzyme. In one of the monomers, this Trp (i.e., Trp42B) would be switching between two χ_1 and χ_2 rotamer states that are not equally perturbed by the presence of nearby Tyr59. In the other monomer, no such flipping between rotamer states would occur, i.e., Trp42 would never be brought into contact with Tyr59. Upon complex formation, the previously interconverting Trp42B would stop its flipping, thus becoming similar to the other one. Experimentally, this interpretation is supported by the small magnitude of the red-shift in the emission spectra of the acrylamide quenching experiments (4 nm) resulting in a 340 nm maximum for the red population, difficult to associate with fully solvated Trp6s, for which we would expect an emission maximum around 348 nm (Lakowicz, 1983). The two populations assigned to the Trp42B rotamers in the apoenzyme would then consist of one rotamer population (the blue one) more exposed to the hydrophobic residues of the protein matrix (Try59B, Leu38B) and the other one, the rotamer population, less exposed to these after the flip (the red one).

Local Trp environment features related to dynamics that support the assignment of Trp fluorescence lifetimes

Known quenchers of Trp fluorescence in model compounds and proteins include the side chains of Lys, Gln, Asn, protonated and unprotonated His, protonated Glu and Asp, Tyr, Cys, and cystine, as well as the peptide bond itself (Vos & Engelborghs, 1994; Chen et al., 1996; Hennecke et al., 1997; Chen & Barkley, 1998; Sillen et al., 2000). We now discuss the possible reasons as to why the lifetime of Trp42B could be shorter than that of Trp42, and how to account for Trp6 and Trp6B.

The Trp42s

The MDS trajectories support the interpretation of two Trp42 populations, in that they identify two groups of Trp42 in terms of their different accessibility to quenching by Tyr59 (cf. Figs. 7–10), which we now discuss. The first Trp42 population consists of Trps that do not come into close contact with this tyrosine during the time course of the simulations, and it consists in the apoenzyme of the g^+ and 90° rotamers of Trp42 and can thus be identified as the long-term component of the decay; the second population consist-

ing of Trp42B that flips between rotamers thus approaching Tyr59 within effective quenching distance. This type of Trp can be identified as the source of the shorter lifetime component. The contribution of each component to the total decay, i.e., 80% for the long and 20% for the short lifetime components, agrees well with this concept. Out of the four Trp42 rotamers in the apoenzyme, three would be in a conformation that never comes into close contact with Tyr59 while the fourth would be spending time between two states, one that overlaps with Tyr59 and one that does not, with the transition between conformers being fully solvent-accessible. The number of Trps accessible for quenching (i.e., of shorter lifetimes) should be less than ~25% of the total. This agrees with our results. In the complex, Trp42B rotamers would no longer come within quenching distance of Tyr59, and they would become similar to the first population.

A note of functional interest here is that the timescale of rotamer interconversion occurs in our trajectories within the timescale of HIV-protease flap opening, as simulated by activated MDS to be possible within ~140 ps (Collins et al., 1995), which leads us to speculate as to whether there could be a possible correlation between Trp42B rotamer interconversion and flap opening. This is supported by recent preliminary anisotropy data (J. Fidy, B. Ulrich, M. Laberge, F. Tolgyesi, L. Polgar, Z. Szeltner, J. Gallay, & M. Vincent, unpubl. data) obtained by synchrotron radiation (LURE, Orsay) and evaluated by MEM analysis. These results showed the presence of sub-ns rotational correlation time constants besides a ~15 ns component attributed to rotation of the whole protein (Eftink, 1983). Similar results were recently published on a slightly different HIV-1 protease system with better resolution in the sub-ns range (Ringhofer et al., 1999). In our preliminary anisotropy experiments, a 10–100 ps broad unresolved envelope of θ-values was seen in the sub-ns range and we inspected the trajectories for dynamic evidence other than the Trp42 rotamer interconversion. We inspected backbone "wobble" rotational motion, defined by changes along the CA-CB-CD axis and associated with the Ramachandran ψ and ϕ angles of the peptide segment near the Trps. Significant "wobble" motion could only be extracted for the backbone region that includes the Trp42s. In the literature, Trp-associated backbone motion has been assigned to the 200 ps or ns rotational correlation time regime, as for example in the case of the Tet repressor, also a homodimer of some ~207 residues (Vergani et al., 2000).

At this point, we speculate that the unresolved ps-timescale anisotropy decay, which our preliminary results yield, encompass the Trp42 rotamer interconversion at the ~50ps "end" of the broad range as well as the above-mentioned backbone "wobble," observed only in the peptide region including the Trp42s. These observations, i.e., evidence for backbone "wobble" in the Trp42 region, its timescale, the timescale of the χ_1/χ_2 rotameric interconversions of these Trps would seem to support such a Trp42/flap opening correlation, and consequently the assignment of the fluorescence lifetime components.

The Trp6s

Unlike the Trp42s, located in the flap region of the protease, which opens by as much as ~7 Å during the inhibitor binding event (Wlodawer & Erickson, 1993), the Trp6s in both apoenzyme and complex are not located in a dynamically active region of the protease. In our model, based on the simulations, the backbone "wobble" motion is insignificant for this region: during the course of the MDS, the Trp6s do not sample different conformations and do not come within contact distance of protein quencher groups. Moreover, their CE3 atoms do not come within efficient peptide carbonyl C quenching distance, i.e., $d_{\text{CE3-C}} < 4.5$ Å. It could be still reasonable to assume that they are even more active than the Trp42s, simply because there is no apparent steric hindrance to the mobility of their indoles. As such, their interconversion could then very well occur on a faster timescale. Inspection of our trajectories, however, could not yield support for this interpretation. The simulations show that wat423 (retained from the initial X-ray structure) simultaneously H-bonds to the NH of adjacent Lys7 and to NH of Trp6. Trp42s do not H-bond with solvent. This tethering of Trp6 to the protein surface would be sufficient to hinder the rotation of Trp6 indoles, by providing a rotational barrier of the order of ~5 kcal mol^{-1}. A similar effect has been modeled for the Trp of phospholipase A to account for experimental anisotropy decays indicative of hindered rotation and it could be seen in the trajectories only with explicit -H simulations, which is also the approach we used. This confers a slightly dipolar character to the indole and allows realistic simulation of H-bonding patterns (Axelsen et al., 1991).

These considerations allow us to possibly account for Trp6s in the model suggested by the simulations, i.e., they would be unable to sample rotameric states with lifetimes distinguishable by their different local environments. In this interpretation, they could be assigned a sub-ns lifetime, with possible quenching either by solvent (Chen & Barkley, 1998) or as a result of efficient nonradiative pathways such as energy transfer or electron transfer. For the latter assignment, we need to postulate the presence of possible electron acceptors in their immediate vicinity. If we compare the respective environments of Trp6s and Trp42s within a 7 Å sphere, we note the following arrangements: for the Trp42s, of eight residues present in the sphere, three are basic (Lys41B, Lys43B, Arg57B) and two are hydrophobic (Tyr59B, Leu38B). It is of interest to note also the presence of three so-called "conformationally important residues," i.e., Pro44B, Gly40B, and Pro39B, highly flexible and undoubtedly required for the flap opening mechanism. In contrast, the five residues facing the Trp6s are: one basic (Lys7) and four polar residues (Thr4B, Gln92, Asn88, and Thr91). This availability of polar groups in the vicinity of the two Trp6s would meet the requirement for the presence of electron acceptors. Reorientational relaxation of any of these residues as a result of the much higher dipole moment of indole in the excited state (Callis, 1997) would yield a sub-ns lifetime for the Trp6s (cf. Hudson et al., 1999 for a discussion of Trp quenching by Gln in bacteriophage T4 lysosyme). However, for such a quenching mechanism to be operative, there is a contact requirement, such as, for example, an H-bond between Trp6 and one of the neighbor Gln or Thr that we do not observe in the 500 ps trajectories. However, we should point out that the length of our simulations is not adequate to fully describe the concerted motions involved in the observed Trp fluorescence processes. The limitations of MDS as applied to systems of the size of proteins are essentially twofold: crude approximations have to be made concerning the interaction potentials and only narrow time windows can be covered. As such, the statistically probable energy fluctuations of the system cannot be adequately sampled (Axelsen et al., 1991).

The other possible Trp6 quenching mechanism could be Förster-type energy transfer. Unfortunately, our present data does not allow the accurate calculation of the proposed energy transfer efficiency because we are lacking the distinct Trp6 overlap inte-

grals. However, inspection of the static X-ray structure shows that the Trp6s are separated by a distance of 25 Å with face-to-face orientation of the indoles (cf. Fig. 2). Using this distance and literature data for a three-Trp protein (De Beuckeleer et al., 1999), we can roughly estimate the transfer efficiency. Supposing an R_0 value of 11–12 Å, the efficiency at a distance of 25 Å would amount to some ~20%, which does not account for a strong quenching effect.

Conclusions

The effect of binding the inhibitor

The present study proposes a model in which the partially solvent-exposed Trp42 in HIV-1 protease, located far from the active site for substrate binding, and also far from the tip of the flap region to feel drastic—and immediately local—structural changes, would still able to report on the conformational effects caused by the binding of the inhibitor acetyl pepstatin. The model suggests that the conformational fluctuations of both Trp42s become restricted upon binding the inhibitor. It is worth mentioning the special efforts required to use the apoenzyme as a reference system for which no reliable structural data were available previously because of the protease autoproteolysis problem. This difficulty was carefully handled in the present work. Also, this work supports the validity of investigating the role of Trp rotamer states in a protease system using a combined molecular dynamics simulations and experimental approach. As such, the study supports models of tryptophan fluorescence based on ground state conformational heterogeneity (Engh et al., 1986; Hutnik & Szabo, 1989; Ross et al., 1992). Furthermore, our interpretation of the lack of Trp6 contribution to the 1–10 ns-timescale fluorescence suggests that the study of quenching processes in some cases definitely requires the use of femtosecond techniques. Finally, in spite of the arduous process involved in trying to account for the proposed non-ns lifetimes of the Trp6s, we believe that we have presented a plausible model for the occurrence of Trp42 rotameric states. The rotational barrier seen in the MDS for the Trp6s is also perhaps suggestive of the attention required to understand quenching mechanisms that are not collisional, i.e., those operating through space (Silva & Prendergast, 1996).

Materials and methods

Sample preparation

HIV-1 protease was expressed in *Escherichia coli* 1458, and purified from inclusion bodies as described previously (Polgár et al., 1994). The enzyme contains three mutation sites at positions 7 (Gln → Lys), 33 (Leu → Ile), and 63 (Leu → Ile). This mutant form of the enzyme is resistant against autodegradation; its kinetic properties and inhibition profiles by a variety of inhibitors, however, were very similar, if not identical with the wild-type enzyme (Mildner et al., 1994). The high similarity of the kinetic properties of the wild-type enzyme and that of the mutant form suggests that the structure of the protein is not changed very much by mutation. The final concentration of the enzyme was 10.6–12.5 μM in 50 mM phosphate buffer containing 50 mM disodium-hydrogen-phosphate, 1 mM EDTA, 2 mM DTE, 0.1 M NaCl, 10 v/v% glycerol, and 0.1% PEG 2000, pH = 7.5, and was used without further dilution. The concentration of the enzyme was determined from the optical density (ϵ_{280} = 25,500 $M^{-1}\,cm^{-1}$) with a Cary 4E (Varian, Australia) UV-VIS spectrophotometer. Aliquots of the concentrated enzyme were stored at −70 °C. The enzyme activity was controlled before the experiments by fluorescence spectroscopy making use of the fluorogenic substrate 2-aminobenzoyl-Thr-Ile-Nle-Phe(NO_2)-Gln-Arg (Szeltner & Polgár, 1996).

Acetyl-pepstatin [Ac-Val-Val-Sta-Ala-Sta], obtained from Sigma Chemicals (St. Louis, Missouri) and dissolved in DMSO, was used as inhibitor. Aliquots of 0.5 or 1.0 mM stock solutions were added to the protein solution; the protein:inhibitor molar ratio was about 1:2; the resultant DMSO content was 4%. The measurements started after 40 min of incubation at room temperature.

Fluorescence measurements

The experiments were carried out using an Edinburgh Analytical Instruments *CD900* luminometer, fitted with a Hamamatsu *R955* PMT as detector. The instrument is equipped with a 75 W xenon lamp for fluorescence spectroscopy; in fluorescence lifetime studies, a *nF900* type flashlamp (40 kHz, 1.5 ns pulse width) was used with a high purity H_2 gas (10 ppm impurity) filling. The individual intensity decay curves were determined using a time-correlated single photon counting method; data were collected over a time period of 10 lifetimes. The excitation wavelength was 295 nm, and emission was typically measured at 340 nm. Both excitation and emission wavelengths were selected by grating monochromators. The decay curves were analysed by iterative reconvolution using discrete exponentials.

Evaluations based on fluorescence intensity data were corrected for the absorption of acrylamide and for protein self-absorption in the 1 mL cuvettes used according to the following formula:

$$I_{corr} = I_{obs} 10^{(OD_{295}/5 + OD_{340})} \quad (2)$$

where I_{corr} is the corrected fluorescence intensity, I_{obs} is the observed fluorescence intensity, OD_{295} and OD_{340} are the optical densities of the sample at 295 nm and at 340 nm, respectively, the volume of cuvettes was 1 mL.

Quenching of fluorescence

Trp accessibility to small solutes was determined using acrilamide, an efficient quencher of Trp fluorescence and selective for surface residues (Eftink & Ghiron, 1981). Five or ten microliter aliquots of 1, 2.5, and 5 M stock solutions of electrophoretic grade acrylamide (Aldrich Chemical Co., Milwaukee, Wisconsin) in 50 mM phosphate buffer (pH: 7.5) were used as quencher up to a concentration of 0.35 M.

Bimolecular collisional quenching constants (k_q) were determined from the equation based on the τ fluorescence lifetime (Equation 3).

$$\frac{\tau_0}{\tau} - 1 = k_q \tau_0 [Q] \quad (3)$$

where $k_q\tau_0 = K_D$, the dynamic quenching constant.

Mean lifetime ($\langle\tau\rangle$) values were obtained from the results of two-component exponential fits according to the formula

$$\langle\tau\rangle = f_1\tau_1 + f_2\tau_2 \quad (4)$$

where f_1 and f_2 are the fractional contributions of τ_1 and τ_2 lifetime components to the total emission, respectively.

Computational methods

The starting coordinates for HIV-1 protease complexed to acetyl-pepstatin (pdb5hvp.ent, 2.0 Å, Fitzgerald et al., 1990) were retrieved from the Brookhaven Protein Data Bank (Bernstein et al., 1977). Residues were replaced as required so as to generate the Q7K/L33I/L63I mutant and the structure was subjected to energy minimization using the *Discover-3* module of the *InsightII* software package (MSI, San Diego California) on a SGI R10000 workstation, with the ESFF force field. Missing hydrogens were added subject to van der Waals constraints and consistent with the ionization state of charged *R* groups at the experimental pH, i.e., 7.5. To remove artifacts due to the addition of explicit hydrogens, energy minimization was performed using a conjugate gradient algorithm until the average (root-mean-square) energy derivative reached 0.1 kcal mol^{-1} A^{-1}. The HIV-1 protease structure without inhibitor was modeled in two different ways, the first using the 2.7 Å structure (pdb3phv.ent, Lapatto et al., 1989) and the second using the available coordinates of the Q7K/L33I/L63I mutant (pdb1a30.ent, 2.0 Å, Louis et al., 1998). The mutant is bound to the Glu-Asp-Leu tripeptide, which was removed prior to generating the fully opened flap structure of the unbound protease. Flap opening was achieved by template forcing the atomic coordinates of the mutant structure of residues 1 to 25 and 65 to 99 in each monomer to the coordinates of the "fully flap-opened" 3phv structure and minimizing as described above, following essentially the approach described by Collins et al. (1995) in their simulation of the protease's flap opening. The stereochemical quality of all structures was verified and corrected using the program PROCHECK 3.4 (Laskowski et al., 1993; Rullman, 1996), which compares a given structure to well-refined structures at the same resolution, thus providing an indication of residue reliability in terms of ideal bond lengths and angles, backbone ϕ and φ torsion angles, and Cα chirality. It was felt that special care had to be paid in generating optimal apoenzyme structures, since our objective was to run dynamics on both complexed and uncomplexed proteases while ensuring that any observed differences in Trp dynamics between them would not be due to structural artefacts and/or poor contacts in the apoenzyme. The apo-HIV protease retained for the simulations were the higher resolution mutated proteases, as PROCHECK consistently returned better stereochemical parameters for these structures. The solvent accessible surface areas (SASA) of the residues—defined as the surface generated by a sphere of the radius of a water molecule of 1.4 Å rolled around the residue (Lee & Richards, 1971)—was calculated using FANTOM (Fraczkiewicz & Braun, 1998). The areas are expressed as ratios of the indole surface area to the random coil value of Trp, defined as the Trp SASA in the tripeptide Gly-Trp-Gly in an ensemble of 30 random conformations. Trp is considered solvent-exposed if $R >$ 50% and buried if $R < 20\%$.

The molecular dynamics simulations were first run with solvated structures. To generate bulk solvent, the structures were explicitly solvated in PBC cell of water molecules (6888 waters), also retaining the water molecules of the X-ray structure. A dielectric constant of 1 was used throughout the simulations. First the 3D solvent cell was equilibrated, holding the protein coordinates fixed, then the entire solvated system was subjected to energy minimization.

NVT simulations were carried out at a constant temperature of 300 K using a leapfrog algorithm with a time step of 1 fs. 200 ps trajectories were acquired, and the initial equilibration 100 ps were disregarded in the analysis. Nonbond interactions were taken into account using the cell multipole method (Schmidt & Lee, 1991) as previously described (Laberge et al., 1998).

As explicitly solvated, dynamics are quite CPU-time consuming; longer 600 ps trajectories were then acquired using the distance-dependent dielectric approximation (Mehler & Solmajer, 1991). As the trajectories of comparable timescales (i.e., 100 ps) yielded the same results as the explicitly solvated runs with respect to Trp dihedral angles, we acquired the longer time simulations with the dd-ϵ approach, thus considered satisfactory.

The Trp indole motion was analyzed by following the variations of the Trp χ_1 and χ_2 dihedral angles. These angles are defined as follows: χ_1 = N-CA-CB-CG and χ_2 = CA-CB-CG-CD2 (IUPAC-IUB Commission on Biochemical Nomenclature, 1970), and we use them as indicators of indole rotation about the CA-CB and CB-CG bonds, respectively (see also Figs. 7, 8). The stereochemically favored rotamers of the χ_1 conformation are the staggered forms, possible when $\chi_1 = 60$, -60, and 180°; these rotamers are called the g^+, g^-, and t rotamers, respectively. Similarly, the favored χ_2 rotamers are the 90° and −90° forms (Szabo & Rayner, 1980; Willis et al., 1994).

Acknowledgments

The authors thank A. Demchenko (Palladin Institute of Biochemistry, Kiev) for valuable suggestions and for reading the manuscript and also W. Braun (UTMB Galveston, Texas) for a copy of his FANTOM program and R.A. Laskowski (UC London, GB) for PROCHECK. The authors also thank J. Gallay and M. Vincent for use of the fluorescence decay facilities at LURE, Orsay (France). M.L. gratefully acknowledges support from Hungarian postdoctoral grant MKM FKFP 1191/1997 (J.F.). B.U. thanks for support from the PhD program no. 11 of the Semmelweis University, Budapest. The technical assistance of Mrs. R. Markács is greatly appreciated.

References

Axelsen PH, Gratton E, Prendergast FG. 1991. Experimentally verufying molecular dynamics simulations through fluorescence anisotropy measurements. *Biochemistry 30*:1173–1179.

Bernstein FC, Koetzle TF, Williams GJB, Meyer EF Jr, Brice MD, Rodgers JR, Kennard O, Shimanouchi T, Tasumi M. 1977. The Protein Data Bank: A computer-based archival file for macromolecular structures. *J Mol Biol 112*:535–549.

Bismuto E, Irace G. 1994. Unfolding pathway of apomyoglobin. Simultaneous characterization of acidic conformational states by frequency domain fluorometry. *J Mol Biol 241*:103–109.

Callis PR. 1997. L_a and L_b transitions of tryptophan: Applications of theory and experimental observations to fluorescence of proteins. *Methods Enzymol 278*:113–150.

Chen Y, Barkley MD. 1998. Toward understanding tryptophan fluorescence in proteins. *Biochemistry 37*:9976–9982.

Chen Y, Liu B, Yu HT, Barkley MD. 1996. The peptide bond quenches indole fluorescence. *J Am Chem Soc 118*:9271–9278.

Collins JR, Burt SK, Erickson JW. 1995. Flap opening in HIV-1 protease simulated by "activated" molecular dynamics. *Struct Biol 2*:334–338.

De Beuckeleer K, Volckaert G, Engelborghs Y. 1999. Time resolved fluorescence and phosphorescence properties of the individual tryptophan residues of Barnase: Evidence for protein-protein interactions. *Proteins Struct Funct Genet 36*:42–53.

Eftink M. 1983. Quenching-resolved emisson anisotropy studies with single and multitryptophan-containing proteins. *Biophys J 43*:323–334.

Eftink MR, Ghiron CA. 1976. Fluorescence quenching of indole and model micelle systems. *J Phys Chem 80*:486–493.

Eftink MR, Ghiron CA. 1981. Fluorescence quenching studies with proteins. *Anal Biochem 114*:199–227.

Engh RA, Chen LXQ, Fleming GR. 1986. Conformational dynamics of tryptophan: A proposal for the origin of the non-exponential fluorescence decay. *Chem Phys Lett 126*:365–372.

Fitzgerald PMD, McKeever BM, VanMiddlesworth JF, Springer JP, Heimbach JC, Leu ChT, Herber WK, Dixon RAF, Darke PL. 1990. Crystallographic analysis of a complex between human immunodeficiency virus type 1 protease and acetyl-pepstatin at 2.0 Å resolution. *J Biol Chem 265*:14209–14219.

Flexner C. 1998. HIV-protease inhibitors. *New Eng J Med 338*:1281–92.

Fraczkiewicz R, Braun W. 1998. A new efficient algorithm for calculating solvent accessible surface areas of macromolecules. *J Comp Chem 19*:319–333.

Hennecke J, Sillen A, Huber-Wunderlich M, Engelborghs Y, Glockshuber R. 1997. Quenching of tryptophan fluorescence by the active-site disulfide bridge in the DsbA protein from *E. coli*. *Biochemistry 36*:6391–6400.

Hutnik CM, Szabo AG. 1989. Confirmation that multiexponential fluorescence decay behavior of holoazurin originates from conformational heterogeneity. *Biochemistry 28*:3923–3934.

Kohl NE, Emini EA, Schleif WA, Davis LJ, Heimbach JC, Dixon RAF, Scolnick EM, Sigal IS. 1988. Active human immunodeficiency virus protease is required for viral infectivity. *Proc Natl Acad Sci USA 85*:4686–4690.

Kungl AJ, Visser NV, van Hoek A, Visser AJWG, Billich A, Schilk A, Gstach H, Auer M. 1998. Time-resolved fluorescence anisotropy of HIV-1 protease inhibitor complexes correlates with inhibitory activity. *Biochemistry 37*:2778–2786.

Laberge M, Vreugdenhill AJ, Vanderkooi J, Butler IS. 1998. Microperoxidase-11: Molecular dynamics and q-band excited resonance raman of the oxidized, reduced and carbonyl forms. *J Biomol Struct Funct 15*:1039–1050.

Lakowicz JR. 1983. *Principles of fluorescence spectroscopy*. New York: Plenum. p 264.

Lapatto R, Blundell T, Hemmings A, Overington J, Wilderspin A, Wood S, Merson JR, Whittle PJ, Danley DE, Geohegan KF, et al. 1989. X-ray analysis of HIV-1 proteinase at 2.7-Å resolution confirms homology among retroviral enzymes. *Nature 342*:299–302.

Laskowski RA, MacArthur MW, Moss DS, Thornthon JM. 1993. PROCHECK: A program to check the stereochemical quality of protein structures. *J Appl Crystallogr 26*:283–291.

Lee B, Richards FM. 1971. The interpretation of protein structures: Estimation of static accessibility. *J Mol Biol 55*:379–400.

Lehrer SS. 1971. Solute perturbation of protein fluorescence. The quenching of the tryptophyl fluorescence of model compounds and of lysozyme by iodide ion. *Biochemistry 10*:3254–3263.

Louis JM, Dyda F, Nashed NT, Kimmel AR, Davies DR. 1998. Hydrophilic peptides derived from the transframe region of gag-pol inhibit the HIV-1 protease. *Biochemistry 37*:2105–2113.

Mehler EL, Solmajer T. 1991. Electrostatic effects in proteins: comparison of dielectric and charge models. *Protein Eng 4*:903–910.

Mildner AM, Rothrock DJ, Leone JW, Bannow CA, Lull JM, Reardon IM, Sarcich JL, Howe WJ, Tomich C-SC, Smith CW, et al. 1994. The HIV-1 protease as enzyme and substrate: Mutagenesis of autolysis sites and generation of a stable mutant with retained kinetic properties. *Biochemistry 33*:9405–9413.

Navia MA, Fitzgerald PMD, McKeever BM, Leu ChT, Heimbach JC, Herber WK, Sigal IS, Darke PL, Springer JP. 1989. Three-dimensional structure of aspartyl-protease from human immunodeficiency virus HIV-1. *Nature 337*:615–620.

Nicholson LK, Yamazaki T, Torchia DA, Grzesiek S, Bax A, Stahl SJ, Kaufman JD, Wingfield PT, Lam PYS, Jadhav PK, et al. 1995. Flexibility and function in HIV-1 protease. *Struct Biol 2*:274–280.

Pargellis ChA, Morelock MM, Graham ET, Kinkade P, Pav S, Lubbe K, Lamarre D, Anderson PC. 1994. Determination of kinetic rate constants for the binding of inhibitors to HIV-1 protease and for the association and dissociation of active homodimer. *Biochemistry 33*:12527–12534.

Polgár L, Szeltner Z, Boros I. 1994. Substrate-dependent mechanisms in the catalysis of human immunodeficiency virus protease. *Biochemistry 33*:9351–9357.

Ringhofer S, Kallen J, Dutzler R, Billich A, Visser AJWG, Scholz D, Steinhauser O, Schreiber H, Auer M, Kungl AJ. 1999. X-ray structure and conformational dynamics of the HIV-I protease in complex with the inhibitor SDZ283-910: Agreement of time-resolved spectroscopy and molecular dynamics simulations. *J Mol Biol 286*:1147–1159.

Rosé JK, Salto R, Craik CS. 1993. Regulation of autoproteolysis of the HIV-1 and HIV-2 proteases with engineered amino acid substitutions. *J Biol Chem 268*:11939–11945.

Ross JBA, Wyssbrod HR, Porter RA, Schwartz GP, Michaels CA, Laws WR. 1992. Correlation of tryptophan fluorescence intensity decay parameters with ^{1}H NMR-determined rotamer conformations: [Tryptophan^2]Oxytoxin. *Biochemistry 31*:1585–1594.

Rullman JAC. 1996. AQUA, Computer program. Department of NMR Spectroscopy, Bijvoet Center for Biomolecular Research, Utrecht University, The Netherlands.

Schmidt KE, Lee MA. 1991. Implementing the fast multipole method in three dimensions. *J Stat Phys 63*:1223–1237.

Seelmeier S, Schmidt H, Turk V, von der Helm K. 1988. Human immunodeficiency virus has an aspartic-type protease that can be inhibited by pepstatin A. *Proc Natl Acad Sci USA 85*:6612–6616.

Sillen A, Diaz JF, Engelborghs Y. 2000. A step toward the prediction of the fluorescence lifetimes of tryptophan residues in proteins based on structural and spectral data. *Protein Sci 9*:158–169.

Silva ND, Prendergast FG. 1996. Tryptophan dynamics of the FK506 binding protein: Time-resolved fluorescence and simulations. *Biophys J 70*:1122–1137.

Szabo AG, Rayner DM. 1980. Fluorescence decay of tryptophan conformers in aqueous solution. *J Am Chem Soc 102*:554–563.

Szeltner Z, Polgár L. 1996. Conformational stability and catalytic activity of HIV-1 protease are both enhanced at high salt concentration. *J Biol Chem 271*:5458–5463.

Tran CD, Beddard GS. 1985. Studies of the fluorescence from tryptophan in melittin. *Eur Biophys J 13*:59–64.

Trylska J, Antosiewicz J, Geller M, Hodge CN, Klabe RM, Head MS, Gilson MK. 1999. Thermodynamic linkage between the binding of protons and inhibitors to HIV-1 protease. *Protein Sci 8*:180–195.

Tyagi SC, Simon SR, Carter CA. 1994. Effect of pH and non physiological salt concentrations on human immunodeficiency virus HIV-1 protease dimerization. *Biochem Cell Biol 72*:175–181.

Valeur B, Weber G. 1977. Resolution of the fluorescence excitation spectrum of indole into the 1La and 1Lb excitation bands. *Photochem Photobiol 25*:441–444.

Vergani B, Kintrup M, Hillen W, Lami H, Piemont E, Bombarda E, Alberti P, Doglia SM, Chabbert M. 2000. Backbone dynamics of Tet repressor a8/a9 loop. *Biochemistry 39*:2759–2768.

Vos R, Engelborghs Y. 1994. A fluorescence study of tryptophan-histidine interaction in the peptide anantin and in solution. *Photochem Photobiol 60*:24–32.

Wang YX, Freedberg DI, Grzesiek S, Torchia DA, Wingfield PT, Kaufman JD, Stahl SJ, Chang ChH, Hodge NC. 1996a. Mapping hydration water molecules in the HIV-1 protease/DMP323 complex in solution by NMR-spectroscopy. *Biochemistry 35*:12694–12704.

Wang YX, Freedberg DI, Yamazaki,T, Wingfield PT, Stahl SJ, Kaufman JD, Kiso Y, Torchia DA. 1996b. Solution NMR evidence that the HIV-1 protease catalytic aspartyl groups have different ionization states in the complex formed with the asymmetric drug KNI-272. *Biochemistry 35*:9945–9950.

Willis KJ, Neugebauer W, Sikorska M, Szabo AG. 1994. Probing α-helical secondary structure at a specific site in model peptides via restriction of tryptophan side-chain rotamer conformation. *Biophys J 66*:1623–1630.

Wlodawer A, Erickson JW. 1993. Structure-based inhibitors of HIV-1 protease. *Annu Rev Biochem 62*:543–585.

Wlodawer A, Miller M, Jaskolski M, Sathyanarayana KB, Baldwin E, Weber TI, Selk ML, Clawson L, Schneider J, Kent HBS. 1989. Conserved folding in retroviral proteases: Crystal structure of a synthetic HIV-1 protease. *Science 245*:616–621.

Wlodawer A, Vondrasek J. 1998. Inhibitors of HIV-1 protease: A major success of structure-assisted drug design. *Annu Rev Biophys Biomol Struct 27*:249–284.

Yamazaki T, Nicholson LK, Torchia DA, Stahl SJ, Kaufman JD, Wingfield PT, Domaille PJ, Campbell-Burk S. 1994. Secondary structure and signal assignments of human-immunodeficiency-virus-1 protease complexed to a novel, structure-based inhibitor. *Eur J Biochem 219*:707–712.

Yengo CM, Chrin L, Rovner AS, Berger CL. 1999. Intrinsic tryptophan fluorescence identifies specific conformational changes at the actomyosin interface upon action binding and ADP release. *Biochemistry 38*:14515–14523.

York DM, Darden TA, Pedersen LG, Anderson MW. 1993. Molecular-dynamic simulation of HIV-1 protease in a crystalline environment and in solution. *Biochemistry 32*:1443–1453.